Pressure-Transient Behavior of Horizontal Wells With and Without Gas Cap or Aquifer

F.J. Kuchuk, SPE, **P.A. Goode,** SPE, **D.J. Wilkinson,** SPE, and **R.K.M. Thambynayagam,*** SPE, Schlumberger-Doll Research

Summary. New analytic solutions are presented in real time and as Laplace transforms for horizontal wells in reservoirs bounded at the top and bottom by horizontal planes. Two types of boundary conditions are considered at these planes, and the Laplace-transform pressure solutions are used to include wellbore-storage and skin effects. Solutions are based on the uniform-flux, line-source solution, but differ from most existing solutions owing to the use of pressure averaging to approximate the infinite-conductivity wellbore condition and use of the correct equivalent wellbore radius for an anisotropic reservoir. New flow periods (regimes) are identified, and simple equations and existence criteria are presented for the various flow periods that can occur during a transient test.

Introduction

Determination of transient pressure behavior for horizontal wells has aroused considerable interest over the past 10 years.[1-4] An extensive literature survey on horizontal wells can be found in Ref. 2. Most work dealing with the horizontal-well problem uses the instantaneous Green's function technique developed by Gringarten and Ramey[5] to solve the 3D isotropic diffusivity equation. Goode and Thambynayagam[2] used finite Fourier transforms to solve the anisotropic problem for the line-source case.

Because the infinite-conductivity inner-boundary condition (uniform pressure over the sandface) poses a very difficult boundary-value problem, a uniform-flux condition on the inner boundary is commonly used. The infinite-conductivity solution is then approximated with either an equivalent-pressure-point or pressure-averaging technique. We prefer the pressure-averaging method because it requires no *a priori* information, is exact in the limit of a small wellbore radius, and is more accurate at intermediate times than the equivalent-pressure-point method. These reasons are discussed further in Appendix A.

Another feature of the solutions presented in this paper is the use of the correct equivalent wellbore radius for an anisotropic formation, which guarantees that elliptical-flow effects near the well are treated correctly at late times. At early times it is preferable to use the elliptical-cylinder solution.[6] Solutions presented in this paper, however, are sufficient for most practical problems.

Using these techniques, we extend the work of Goode and Thambynayagam[2] and Clonts and Ramey[3] to obtain new analytic solutions for horizontal wells with and without the effects of gas cap or aquifer. The wellbore-storage effect is accounted for, and new formulas are presented for the determination of reservoir parameters from the characteristics of different flow regimes.

Solutions With and Without Gas Cap or Aquifer

First we discuss the basic solutions for horizontal wells for the constant-rate case without wellbore-storage and skin effects. These solutions will then be combined with constant wellbore storage and/or measured downhole flow rate.

The horizontal well shown in **Fig. 1** is considered to be completed in an infinite anisotropic medium bounded above and below by horizontal planes. The boundaries of the reservoir in the horizontal directions are considered to be so far away that they are not seen during the test. The permeabilities in the principal directions are denoted by k_x, k_y, and k_z. We develop the solutions for the general case where the three permeabilities are all different in Appendices A and B, but in the text we consider a transversely isotropic medium and write $k_x=k_y=k_H$ and $k_z=k_V$. The flow of a slightly compressible fluid of constant compressibility and viscosity is assumed throughout the medium. Gravity effects are neglected. Two types of top and bottom boundary conditions are considered. In the first case, both the top and the bottom boundaries have no-flow conditions. In the second case, one of the boundaries is at constant pressure, while the other is a no-flow boundary as before; this case can represent either a gas cap at the top boundary or an active aquifer (in which the water mobility is high compared with the mobility of the reservoir fluid) at the bottom. For convenience, we refer to the first model as the no-flow-boundary model and to the second as the constant-pressure-boundary model. The notation of this paper assumes that in the latter model, the constant-pressure boundary is at the top (the gas-cap case), but the formulas may be readily adapted for the case of an aquifer at the bottom.

During the last few years, several solutions for horizontal wells have been presented.[1-4] Most of these solutions are for the no-flow-boundary model, and apart from the work of Goode and Thambynayagam,[2] none present solutions in the Laplace-transform domain. A solution for the constant-pressure condition at both the top and bottom boundaries was presented by Daviau *et al.*[1] This solution is different from the constant-pressure-boundary solution presented here, in which one of the boundaries (top or bottom) is no-flow. This flexibility is important because if we have a constant-pressure boundary such as a gas cap, the well is usually drilled close to the other (no-flow) boundary.

The solution method is discussed in Appendix A, and the actual solutions are developed in Appendix B. Our solutions differ somewhat from other solutions given in the literature because we approximate the infinite-conductivity condition by averaging the pressure along the well length instead of using an equivalent pressure point. A discussion of the pressure-averaging technique is given in Appendix A, together with a derivation of the correct equivalent wellbore radius to be used for an anisotropic formation.

We define dimensionless time and pressure (in field units) by

$$t_D=0.0002637k_Ht/\phi\mu c_tL_{1/2}^2 \quad \ldots\ldots (1)$$

and $$p_D=(k_Hh/141.2q\mu)[p_i-p_{wf}(t)], \quad \ldots\ldots (2)$$

and other dimensionless parameters

$$h_D=\sqrt{k_H/k_V}\,(h/L_{1/2}), \quad \ldots\ldots (3a)$$

$$z_{wD}=\sqrt{k_H/k_V}\,(z_w/L_{1/2}), \quad \ldots\ldots (3b)$$

and $$r_{wD}=(r_w/2L_{1/2})(1+\sqrt{k_H/k_V}). \quad \ldots\ldots (3c)$$

In the time domain, the dimensionless pressure response, p_D, for constant-rate drawdown is most conveniently given as a time integral over the instantaneous Green's function (see Appendix B):

$$p_D(t_D)=2\pi h_D\int_0^{t_D} d\tau G_x(\tau)G_y(\tau)G_z(\tau), \quad \ldots\ldots (4)$$

where $$G_x(\tau)=\tfrac{1}{2}\{\mathrm{erf}(1/\sqrt{\tau})+\sqrt{\tau/\pi}\,[\exp(-1/\tau)-1]\}, \quad \ldots\ldots (5)$$

$$G_y(\tau)=1/2\sqrt{\pi\tau}, \quad \ldots\ldots (6)$$

*Now at Schlumberger Well Services.

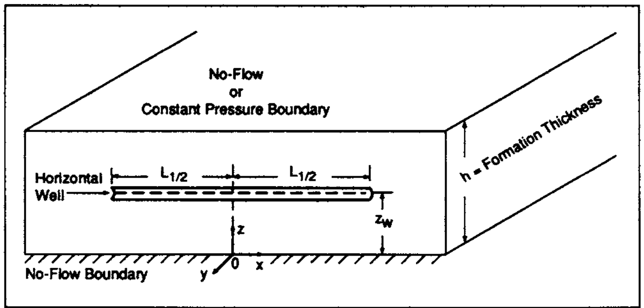

Fig. 1—Horizontal-well model.

TABLE 1—RESERVOIR PARAMETERS FOR EXAMPLES

	Examples				
	1	2	3	4	5
k_x, md	100	100	100	100	200
k_z, md	10	1	5	5	1
$L_{1/2}$, ft	500	500	500	500	500
h, ft	100	100	100	40	200
z_w, ft	20	20	5	20	20
h_D	0.63240	2.0	0.89443	0.35777	5.65685
z_{wD}	0.12649	0.4	0.04472	0.17889	0.56569
r_{wD}	0.00146	0.00389	0.001937	0.00197	0.00530

and $$G_z(\tau)=\frac{1}{h_D}\left[1+2\sum_{n=1}^{\infty}\cos\frac{n\pi z_D}{h_D}\cos\frac{n\pi z_{wD}}{h_D}\exp\frac{-n^2\pi^2\tau}{h_D^2}\right] \quad (7)$$

for the no-flow upper-boundary case, and

$$G_z(\tau)=\frac{2}{h_D}\sum_{n=1}^{\infty}\cos\frac{(n-\frac{1}{2})\pi z_D}{h_D}\cos\frac{(n-\frac{1}{2})\pi z_{wD}}{h_D}\times\exp\frac{-(n-\frac{1}{2})^2\pi^2\tau}{h_D^2} \quad (8)$$

for the constant-pressure upper-boundary case. In both Eqs. 7 and 8, the pressure is evaluated at $z_D=z_{wD}+r_{wD}$.

The Laplace-domain form of the solution is given in Appendix B. We define a function $F(\beta)$ by

$$F(\beta)=\int_0^{\infty}du\frac{\sin^2(u)}{u^2\sqrt{u^2+\beta}} \quad (9)$$

Then, $$\bar{p}_D(s_D)=\frac{1}{s_D}\left[F(s_D)+2\sum_{j=1}^{\infty}F(\xi_j)\cos\frac{j\pi z_D}{h_D}\cos\frac{j\pi z_{wD}}{h_D}\right], \quad (10)$$

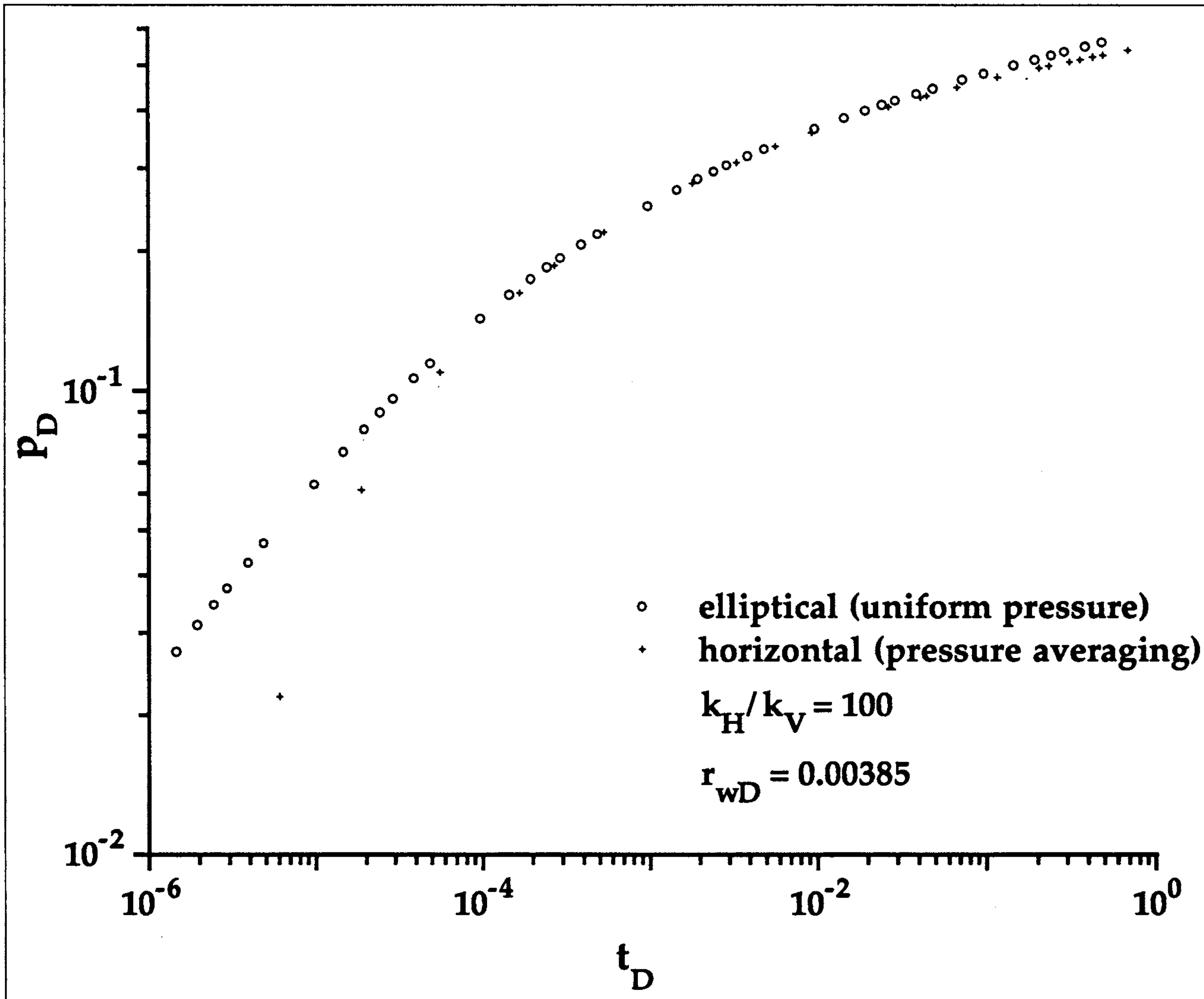

Fig. 2—Comparison of dimensionless pressure from an elliptical and a horizontal well.

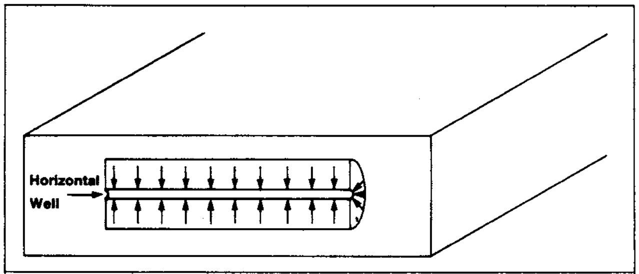

Fig. 3—First early-time radial flow (after Ref. 2).

where $\xi_j = s_D + (j\pi/h_D)^2$ for the no-flow-boundary case, and

$$\hat{p}_D(s_D) = \frac{2}{s_D} \sum_{j=1}^{\infty} \left[F(\xi_j) \cos \frac{(j-½)\pi z_D}{h_D} \cos \frac{(j-½)\pi z_{wD}}{h_D} \right], \quad (11)$$

where $\xi_j = s_D + [(j-½)\pi/h_D]^2$ for the constant-pressure-boundary case. Again, the value of z_D is evaluated at $z_{wD}+r_{wD}$. The dimensionless Laplace variable, s_D, is defined as

$$s_D = \phi\mu c_t L_{½}^2 s/0.0002637k_H. \quad (12)$$

As seen from the above equations, the dimensionless pressure at the wellbore is a function of t_D, h_D, z_{wD}, and r_{wD}. Because we use the line-source approximation, Eqs. 4, 10, and 11 are valid only when $t_D/r_{wD}^2 > 25$. This is an important limitation because for large anisotropy ($k_H/k_V \gg 1$), it may take more than several seconds to satisfy this condition. For smaller t_D, the true behavior is elliptical flow in the *y-z* plane; transient solutions for elliptic flow are given in Ref. 6. **Fig. 2** compares p_D values from Eq. 10 with those from Table 1 in Ref. 6 for $k_H/k_V = 100$. Note that the horizontal-well solution for this high-anisotropy case is inaccurate when $t_D < 0.001$. Also, the solutions deviate from each other after $t_D > 0.1$, at which time the contributions of flow from beyond the ends of the horizontal well start affecting the pressure behavior.

Flow Periods

The duration of the flow periods (regimes) is discussed in detail in Refs. 1 through 4. In this paper, we closely examine some of these flow regimes. In a given test, only one or more flow regimes may develop because of the usually small vertical permeability, which causes the pressure pulse to propagate slowly in the vertical (z) direction. This can result in hours of testing time before the effect of the top and bottom boundaries is observed. Using five synthetic examples, we will show the various flow periods that can occur during the pressure testing of horizontal wells. The values of h_D, z_{wD}, r_{wD}, and other parameters are given in **Table 1**.

Early-Time Radial Flow Periods. ***First Radial Flow Period.*** As discussed above, the very first flow pattern for horizontal wells is elliptic cylindrical. After some time, the elliptic-cylindrical flow period becomes approximately radial, as shown in **Fig. 3**. The derivatives for Examples 1, 3, and 4 **(Fig. 4)** clearly indicate the first radial flow period, which is equivalent to a fully penetrating, vertical well in an infinite reservoir. The asymptotic behavior of the first radial flow period can be obtained from the derivative[7,8] of the dimensionless pressure given by Eq. 4 if $t_D \ll 1$ and $t_D \ll \min\{z_{wD}^2, (h_D - z_{wD})^2\}$, provided that $t_D/r_{wD}^2 > 25$, as

$$\frac{dp_D}{d\ln(t_D)} \approx \frac{h_D}{4}\left\{1 - \sqrt{\frac{t_D}{\pi}} + \exp\left(-\frac{z_{wD}^2}{t_D}\right) \pm \exp\left[-\frac{(h_D - z_{wD})^2}{t_D}\right]\right\}. \quad (13)$$

The $\pm$ sign in Eq. 13 corresponds to the no-flow (+) and constant-pressure (−) boundary models, respectively. In Eq. 13, the correction terms on the first line result from the effects of flow at the well ends, while those in the second line result from the upper and lower boundaries. As discussed in Appendix A, the term $\sqrt{t_D/\pi}$ (representing flow spreading from the ends of the well) results from the pressure-averaging formalism and implies an earlier end to the first radial flow period than the corresponding pressure-point expression.

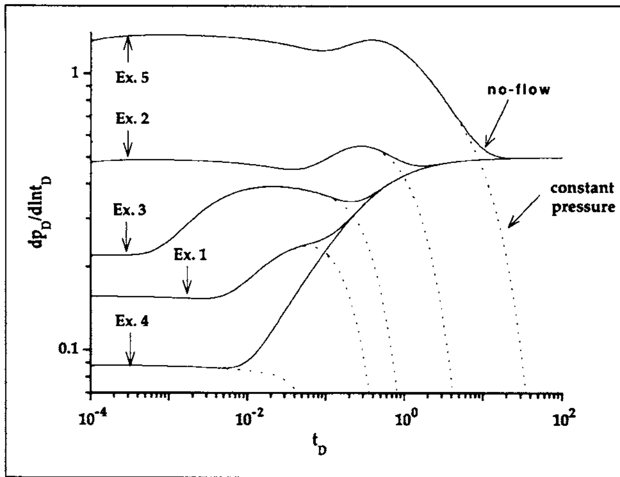

Fig. 4—Dimensionless pressure derivative for Examples 1 through 5.

For a large anisotropy ratio, k_H/k_V, the first radial flow period may not develop because r_{wD} increases and the conditions $t_D/r_{wD}^2 > 25$ (required for pseudosteady flow near the well) and $t_D \ll 1$ (required for the effects of the well ends to be negligible) cannot be satisfied simultaneously. Note that the first effects of the well end develop earlier in the pressure-averaging formalism than in the usual pressure-point method (see Appendix A). The first radial flow period will most definitely end when the effect of the nearest boundary is felt at the wellbore (and, as explained above, may end earlier).

If it exists, the equation for the first radial flow period in oilfield units may be written as

$$p_i - p_{wf} \approx \frac{162.6q\mu}{2\sqrt{k_H k_V} L_{½}} \left[\log\left(\frac{\sqrt{k_H k_V}\, t}{\phi\mu c_t r_w^2}\right) - 3.2275 + 0.8686S - 2\log\frac{1}{2}\left(\sqrt[4]{\frac{k_H}{k_V}} + \sqrt[4]{\frac{k_V}{k_H}}\right)\right], \quad (14)$$

where we include the effect of a damage skin, S, defined with respect to the length of the well. In principle, the geometric mean permeability, $\sqrt{k_H k_V}$, may be obtained from the semilog analysis of the pressure data with Eq. 14, provided that the wellbore pressure during this period is not affected by wellbore storage. For the calculation of damage skin from Eq. 14, we need to know the anisotropy ratio. Because the dependence on $\sqrt{k_H/k_V}$ is logarithmic, however, its effect on the damage skin will usually be small.

The vertical permeability may be obtained from the time of onset of the deviation of the pressure or pressure derivative from the above equations; i.e., when the effect of either the top or bottom boundary is felt at the wellbore. The start of the effect of the nearest boundary (no-flow or constant-pressure) is given by

$$t_D \approx (1/\pi)\min\{z_{wD}^2, (h_D - z_{wD})^2\} \quad (15)$$

and by $t_D \approx (1/\pi)\max\{z_{wD}^2, (h_D - z_{wD})^2\}$ ......(16)

for the other boundary.

Thus, from Eqs. 15 and 16 the vertical permeability (in oilfield units) may be determined by

$$k_V = (\phi\mu c_t/0.0002637\pi t_{snbe})\min\{z_w^2, (h - z_w)^2\}, \quad (17)$$

where t_{snbe} is the time to feel the effect of the nearest boundary, or

$$k_V=(\phi\mu c_t/0.0002637\pi t_{snbe})\max\{z_w^2,(h-z_w)^2\}, \quad \ldots\ldots (18)$$

where t_{sfbe} is the time to feel the second (farthest) boundary effect.

Alternatively, because Eqs. 17 and 18 provide two pieces of information, they may be used to provide constraints on the boundary positions. This could be very useful for the situation where one of the boundary locations changes with time, such as when the gas cap is moving down or there is an unknown continuous shale above or below the well.

Second Radial Flow Period. This is a semicylindrical flow period that follows the first radial flow period and may occur when the well is near a no-flow boundary. For convenience, we will consider the case of the lower boundary. Then, provided that $z_{wD}\ll 1$ and $z_{wD}\ll h_D-z_{wD}$, the semicylindrical flow period will occur for dimensionless times in the range $z_{wD}^2\ll t_D\ll \min[1,(h_D-z_{wD})^2]$.

The equation for the second flow period is similar to Eq. 14; i.e.,

$$p_i-p_{wf}\approx\frac{162.6q\mu}{\sqrt{k_Hk_V}L_{1/2}}\left\{\log\left(\frac{\sqrt{k_Hk_V}\,t}{\phi\mu c_t r_w^2}\right)-3.2275+0.4343S-\log\left[\left(1+\sqrt{\frac{k_H}{k_V}}\right)\frac{z_w}{r_w}\right]\right\}. \quad \ldots\ldots (19)$$

Note that the slope of the semilog straight line of Eq. 19 is twice that of Eq. 14. It also includes a pseudoskin because of the early-time flow period between the well and the nearest boundary. As in the first radial flow period, the geometric mean permeability, $\sqrt{k_Hk_V}$, may be obtained from this flow regime.

Intermediate-Time Linear Flow. A horizontal well is generally long compared with the formation thickness. As a result, for the no-flow boundary model, a period of linear flow may develop once the pressure transient reaches the upper and lower boundaries. During this period, the effect of flow at the well ends is negligible compared with that of the overall length of the well. The asymptotic behavior of this period can be obtained from the derivative of the dimensionless pressure given by Eq. 4 if $h_D^2\ll t_D\ll 1$ as

$$\frac{dp_D}{d\sqrt{t_D}}\approx\sqrt{\pi}\left[1-\sqrt{\frac{t_D}{\pi}}+2\cos^2\left(\frac{\pi z_{wD}}{h_D}\right)\exp\left(-\frac{\pi^2t_D}{h_D^2}\right)+2\cos^2\left(\frac{2\pi z_{wD}}{h_D}\right)\exp\left(-\frac{4\pi^2t_D}{h_D^2}\right)\right]. \quad \ldots\ldots (20)$$

Note that if h_D is not small, then the linear flow period will not exist because the flow will spread out significantly from the well ends before the effects of the top and bottom boundaries are seen. Again, the term $\sqrt{t_D/\pi}$ implies an earlier end to the linear flow period than the corresponding pressure-point expression. If we are able to identify this regime, the equation in oilfield units is

$$p_i-p_{wf}\approx\frac{8.128q}{2L_{1/2}h}\sqrt{\frac{\mu t}{k_H\phi c_t}}+\frac{141.2q\mu}{k_Hh}S_z+\frac{70.6q\mu}{L_{1/2}\sqrt{k_Hk_V}}S, \quad \ldots\ldots (21)$$

where the pseudoskin S_z may be visualized as the skin resulting from partial penetration in the vertical direction, given by

$$S_z\approx -1.1513\sqrt{\frac{k_H}{k_V}}\frac{h}{L_{1/2}}\log\left[\frac{\pi r_w}{h}\left(1+\sqrt{\frac{k_V}{k_H}}\right)\sin\left(\frac{\pi z_w}{h}\right)\right]. \quad \ldots\ldots (22)$$

This flow period will not appear for wells with a gas cap or an aquifer.

Late-Time Radial Flow. After a sufficiently long time, the pressure front will become approximately radial in the x-y plane and a third radial flow pattern will develop (see Fig. 4). This period will not exist for wells with a gas cap or aquifer. The asymptotic behavior of this period can be obtained from the derivative of the dimensionless pressure given by Eq. 4 if $t_D\gg 1$ and $t_D\gg h_D^2$ as

$$\frac{dp_D}{d\ln(t_D)}\approx\frac{1}{2}\left[1-\frac{1}{6t_D}+2\cos^2\left(\frac{\pi z_{wD}}{h_D}\right)\exp\left(-\frac{\pi^2t_D}{h_D^2}\right)+2\cos^2\left(\frac{2\pi z_{wD}}{h_D}\right)\exp\left(-\frac{4\pi^2t_D}{h_D^2}\right)\right]. \quad \ldots\ldots (23)$$

Eq. 23 indicates that to see this radial flow period, we must have both $t_D\gg 1$ (so that the pressure pulse has traveled far compared with the well length) and $t_D\gg h_D^2$ (so that the effect of the upper and lower boundaries are fully seen). When $h_D\leq 1$ (which is typically the situation, except for very high anisotropy), the main departure from radial flow will result from the term $1/(6t_D)$. In this case, we estimate the dimensionless time of the onset of radial flow as

$$t_D\approx 20. \quad \ldots\ldots (24)$$

For a large anisotropy ratio, h_D may become large and the start of the radial flow period could be much later than that provided by Eq. 24.

The equation for this radial flow period in oilfield units is

$$p_i-p_{wf}\approx\frac{162.6q\mu}{k_Hh}\left[\log\left(\frac{k_Ht}{\phi\mu c_tL_{1/2}^2}\right)-2.5267\right]+\frac{141.2q\mu}{k_Hh}S_z+\frac{70.6q\mu}{L_{1/2}\sqrt{k_Hk_V}}S, \quad \ldots\ldots (25)$$

where $S_z\approx -1.1513\sqrt{\frac{k_H}{k_V}}\frac{h}{L_{1/2}}\log\left[\frac{\pi r_w}{h}\left(1+\sqrt{\frac{k_V}{k_H}}\right)\sin\left(\frac{\pi z_w}{h}\right)\right]$

$$-0.5\frac{k_H}{k_V}\frac{h^2}{L_{1/2}^2}\left(\frac{1}{3}-\frac{z_w}{h}+\frac{z_w^2}{h^2}\right). \quad \ldots\ldots (26)$$

Eq. 26 is satisfactory if $h_D\leq 5$. If this condition is not satisfied, the full expression (Eq. B-19) must be used. Although it may take many hours to reach the semilog straight line described by Eq. 25, in principle k_Hh can be calculated from the slope.

Steady-State Flow Period. In the constant-pressure model where there is a gas cap or an aquifer at one of the boundaries, intermediate-time linear flow and late-time radial flow periods do not exist; instead, the flow becomes steady state. In Appendix B, we derive an approximate formula (valid for $h_D\leq 2.5$) for the steady-state pressure. In oilfield units this becomes

$$p_i-p_{wf}\approx\frac{162.6q\mu}{\sqrt{k_Hk_V}L_{1/2}}\left\{\log\left[\frac{8h}{\pi r_w(1+\sqrt{k_V/k_H})}\cot\left(\frac{\pi z_w}{2h}\right)\right]+0.4343\left[S-\frac{(h-z_w)}{L_{1/2}}\sqrt{\frac{k_H}{k_V}}\right]\right\}. \quad \ldots\ldots (27)$$

If $h_D>2.5$, this approximation will not provide sufficient accuracy and the full form of the solution (Eq. B-21) must be used. The formation height may be estimated from the time at which the wellbore pressure becomes equal to the steady-state value:

$$h\approx 0.01\sqrt{k_V\,t_{cbp}/\phi\mu c_t}. \quad \ldots\ldots (28)$$

Alternatively, if h is known, Eq. 28 can be used to estimate k_V.

Downhole Pressure Response

Because the early-time interpretation is important to obtain vertical and horizontal permeabilities, it is desirable to reduce wellbore-storage effects by either measuring the downhole flow rate or using

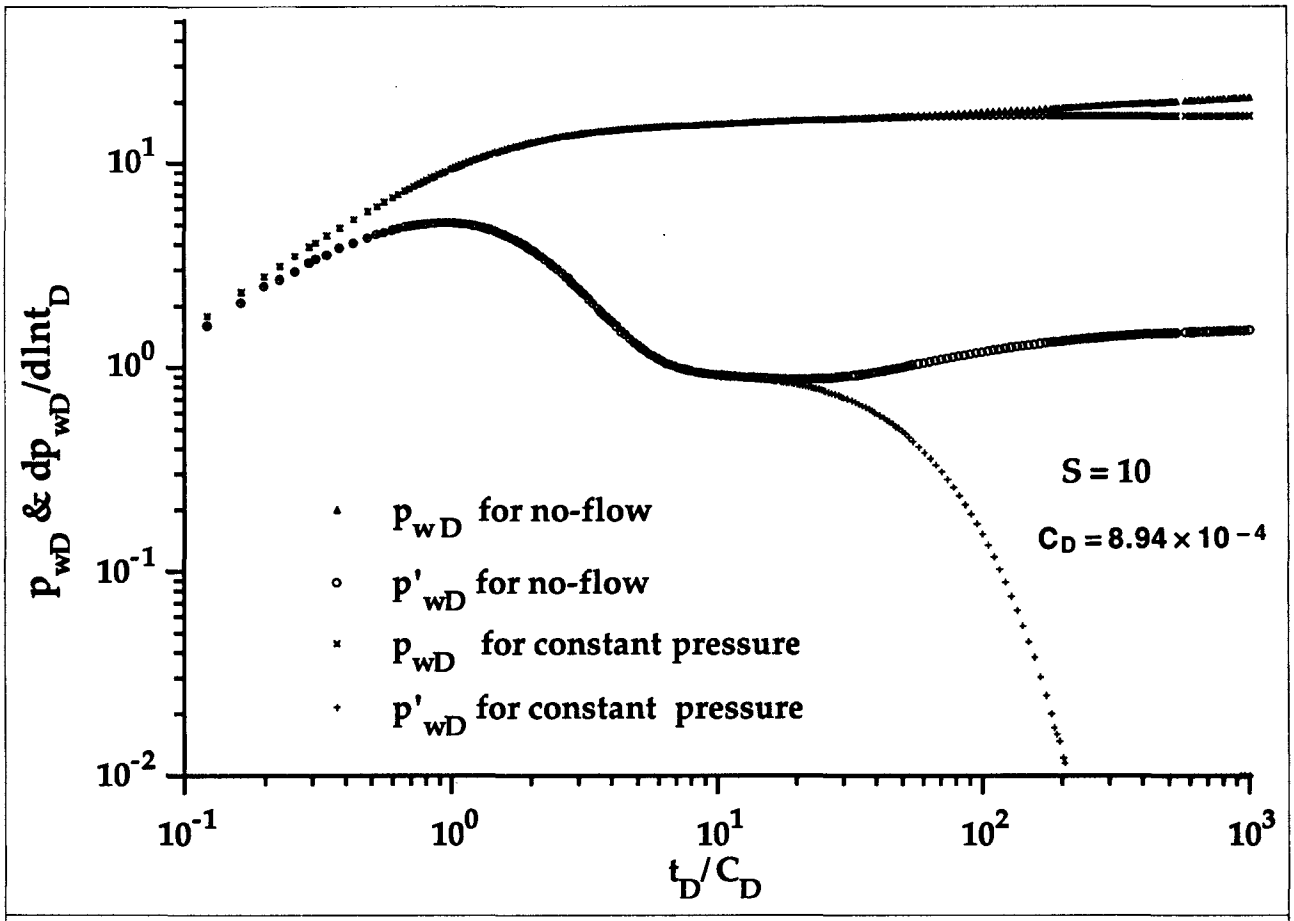

Fig. 5—Dimensionless wellbore pressures and their derivatives with constant wellbore-storage and skin effects for Example 1.

a downhole shut-in tool. Furthermore, if wellbore storage is limited to the wellbore volume between the downhole gauge and the sandface, the usual assumption of a single-phase, constant-storage model is better justified. Even when downhole measurement or shut-in is used, however, there will still be considerable wellbore volume below the tool,[9,10] and the storage effects resulting from this volume typically last longer than those for a vertical well in the same formation because the anisotropy reduces the effective permeability at early times to $\sqrt{k_H k_V}$.

The dimensionless wellbore pressure in terms of the measured flow rate and the wellbore storage resulting from the wellbore volume below the measurement point is given by

$$p_{wD}(t_D)=\int_0^{t_D}\left[q_{mD}(\tau)-C_D\frac{dp_{wD}(\tau)}{d\tau}\right]p'_{SD}(t_D-\tau)d\tau, \quad \ldots\ldots (29)$$

where p_{wD} is nondimensionalized by a constant reference flow rate q_r, and q_{mD} is given in terms of the measured flow rate q_m by q_m/q_r. In Eq. 29, the derivative of the constant-rate response with skin is given by

$$p'_{SD}(t)=p'_D(t)+(h_D/2)S\delta(t). \quad \ldots\ldots (30)$$

In the Laplace domain Eq. 29 becomes

$$\hat{p}_{wD}(s_D)=s_D\hat{q}_{mD}(s_D)\left[\frac{\hat{p}_{SD}(s_D)}{1+C_D s_D^2\hat{p}_{SD}(s_D)}\right], \quad \ldots\ldots (31)$$

where $\hat{p}_{SD}(s_D)=\hat{p}_D(s_D)+(h_D/2)S, \quad \ldots\ldots (32)$

and $\hat{p}_D$ is given by Eqs. 4, 10, and 11. The dimensionless storage coefficient is

$$C_D=5.615C/2\pi\phi c_t h L_{\frac{1}{2}}^2, \quad \ldots\ldots (33)$$

where C is defined with the wellbore volume below the measuring point. If q_m is measured at the wellhead and is constant, Eq. 29 becomes the well-known wellbore-pressure solution with storage and skin[9,10]:

$$p_{wD}(t_D)=\int_0^{t_D}\left[1-C_D\frac{dp_{wD}(\tau)}{d\tau}\right]p'_{SD}(t_D-\tau)d\tau, \quad \ldots\ldots (34)$$

and its Laplace transform is

$$\hat{p}_{wD}(s_D)=\frac{\hat{p}_{SD}(s_D)}{1+C_D s_D^2\hat{p}_{SD}(s_D)}, \quad \ldots\ldots (35)$$

where now C_D is defined by the total wellbore volume, and p_{wD} is nondimensionalized from the constant rate q_m.

The convolution integral (Eq. 29) or its Laplace transform (Eq. 31) provides a general framework for the solution of time-dependent internal-boundary conditions. Eq. 34 or 35 should be used if the downhole flow rate is not measured. The wellbore pressure, p_{wD}, for horizontal wells with wellbore-storage and skin effects was first numerically computed by Daviau *et al.*[1] from Eq. 34 with the numerical wellbore-storage model of Cinco-Ley and Samaniego-V.[10] The computation of p_{wD} from Eq. 34, however, takes much more computer time than from Eq. 35 because Eq. 34 is of convolution type; in other words, for a given time, p_{wD} is always computed starting from $t_D=0$. In addition, as shown by Kuchuk,[11] the error in p_{wD} when computed from Eq. 34 could be as high as 1%.

Fig. 5 presents a log-log plot of the dimensionless wellbore pressure, p_{wD}, and its derivatives with respect to ln t_D for Example 1 ($h_D=0.63240$ and $z_{wD}=0.12649$) with and without a gas cap. Fig. 5 shows that a very pronounced difference exists between the dimensionless pressure or its derivative with and without the gas-cap effect. Fig. 5 also shows that the effect of the lower no-flow boundary (in this case it is closer to the wellbore than the gas cap) is masked by the wellbore-storage effect. Thus, identification of the no-flow boundary from pressure, or its derivative, appears

difficult when wellbore storage dominates. In this situation, the presence of a no-flow boundary and its distance from the wellbore have to be known independently for a unique interpretation of the transient well-test data.

Conclusions

New analytic solutions are presented in real time and in the form of Laplace transforms for horizontal wells bounded by two horizontal boundary planes at the top and bottom. Two boundary conditions are considered. In the first case, both the top and bottom boundaries were impermeable (no-flow condition). In the second case, either one of the boundaries was at constant pressure (the system either had a gas cap or an active aquifer) while the other was a no-flow boundary, as before.

Although we use the uniform-flux line-source solution, like other authors, our results differ somewhat from those appearing in the literature because we estimate the pressure response at the well by averaging the pressure along the well length rather than by using an equivalent pressure point. This technique is believed[12] to be exact at all times in the limit of vanishing wellbore radius and gives a better indication of the way in which flow near the well ends affects the various flow regimes. In addition, we identified the correct equivalent wellbore radius to be used in the case of an anisotropic formation.

New flow periods (regimes) are identified, and simple equations and existence criteria are presented for flow periods that can occur during the course of a transient test. Although the late-time radial flow period for horizontal wells is analogous to the infinite-acting period for vertical wells, the fact that this regime may not develop in a reasonable testing time makes interpretation difficult. A large anisotropy ratio and the potential existence of multiple boundaries at unknown distances from the wellbore also increase the complexity of the interpretation.

These new solutions can be applied to drawdown and buildup tests from horizontal wells with and without a constant-pressure boundary, and the Laplace-domain form of the solutions can be used to obtain solutions that include wellbore-storage and skin effects. With these solutions, it is possible, in principle, to develop pressure and pressure-derivative type curves for different horizontal-well parameters. It is better to use nonlinear least-squares estimation methods (automated type-curve matching), however, to analyze well-test data because of the large number of parameters. For this reason, the efficient computer implementation of the solutions is an important feature of this work.

Nomenclature

a = vertical axis of equivalent elliptical well, ft [m]
b = horizontal axis of equivalent elliptical well, ft [m]
c_t = total compressibility, atm^{-1} [Pa^{-1}]
C = wellbore-storage coefficient, RB-psi^{-1} [m^3·Pa^{-1}]
$F(\beta)$ = function defined by Eq. 9
G = Green's function
h = reservoir thickness, ft [m]
k = permeability, md [m^2]
K_0 = modified Bessel function of second kind, zero order
K_{i2} = second integral of K_0
L = well length, ft [m]
m = Fourier transform variable
n = Fourier transform variable
p = pressure, psi [Pa]
Δp = pressure drop, psi [Pa]
q = volumetric flow rate, B/D [m^3/s]
q_r = constant reference flow rate, B/D [m^3/s]
r = radius, ft [m]
s = dimensionless Laplace transform variable
S = skin
t = time, hours [seconds]
u = integration variable
x,y,z = Cartesian coordinates, ft [m]
γ = Euler's constant=0.577215
$\delta(t)$ = Dirac delta function
μ = viscosity, cp [Pa·s]
ξ_j = dummy variable
τ = dummy variable
ϕ = porosity, fraction

Subscripts

cbp = time to reach steady state
D = dimensionless
H = horizontal
i = initial
m = measured
$sfbe$ = time to feel far boundary
$snbe$ = time to feel near boundary
ss = steady state
V = vertical
w = well
wf = flowing pressure (drawdown)
x,y,z = coordinate indicators
$\frac{1}{2}$ = half

Superscripts

$\hat{}$ = Laplace image plane
$*$ = pressure point coordinate
$'$ = time derivative

References

1. Daviau, F. *et al.*: "Pressure Analysis for Horizontal Wells," *SPEFE* (Dec. 1988) 716–24.
2. Goode, P.A. and Thambynayagam, R.K.M.: "Pressure Drawdown and Buildup Analysis of Horizontal Wells in Anisotropic Media," *SPEFE* (Dec. 1987) 683–97; *Trans.*, AIME, **283**.
3. Clonts, M.D. and Ramey, H.J. Jr.: "Pressure-Transient Analysis for Wells With Horizontal Drainholes," paper SPE 15116 presented at the 1986 SPE California Regional Meeting, Oakland, April 2–4.
4. Ozkan, E., Raghavan, R., and Joshi, S.D.: "Horizontal-Well Pressure Analysis," *SPEFE* (Dec. 1989) 567–75; *Trans.*, AIME, **287**.
5. Gringarten, A.C. and Ramey, H.J. Jr.: "The Use of Source and Green's Functions in Solving Unsteady-Flow Problems in Reservoirs," *SPEJ* (Oct. 1973) 285–96; *Trans.*, AIME, **255**.
6. Kucuk, F. and Brigham, W.E.: "Transient Flow in Elliptical Systems," *SPEJ* (Dec. 1979) 401–10; *Trans.*, AIME, **267**.
7. Tiab, D. and Kumar, A.: "Application of the p'_D Function to Interference Analysis," *JPT* (Aug. 1980) 1465–70.
8. Bourdet, D. *et al.*: "A New Set of Type Curves Simplifies Well Test Analysis," *World Oil* (May 1983).
9. Agarwal, R.G., Al-Hussainy, R., and Ramey, H.J. Jr.: "An Investigation of Wellbore Storage and Skin Effect in Unsteady Liquid Flow: 1. Analytical Treatment," *SPEJ* (Sept. 1970) 279–90; *Trans.*, AIME, **249**.
10. Cinco-Ley, H. and Samaniego-V., F.: "Effect of Wellbore Storage and Damage on the Transient Pressure Behavior of Vertically Fractured Wells," paper SPE 6752 presented at the 1977 SPE Annual Technical Conference and Exhibition, Denver, Oct. 9–12.
11. Kuchuk, F.J.: "Generalized Transient Pressure Solutions With Wellbore Storage," paper SPE 15671, available from SPE Book Order Dept., Richardson, TX (1986).
12. Wilkinson, D.J. and Hammond, P.: "A Perturbation Method for Mixed Boundary Value Problems in Pressure Transient Testing," *Transport in Porous Media* (1990) **5**, 609–36.
13. Muskat, M.: *The Flow of Homogeneous Fluids Through Porous Media*, McGraw-Hill Book Co. Inc., New York City (1937).
14. Gringarten, A.C., and Ramey, H.J. Jr.: "An Approximate Infinite Conductivity Solution for a Partially Penetrating Line-Source Well," *SPEJ* (April 1975) 140–48; *Trans.*, AIME, **259**.

Appendix A–Theoretical Considerations

We use dimensionless variables (written in consistent units).

$$x_D = x/L_{\frac{1}{2}}, \quad \text{(A-1a)}$$

$$y_D = \sqrt{k_x/k_y}\,(y/L_{\frac{1}{2}}), \quad \text{(A-1b)}$$

and

$$z_D = \sqrt{k_x/k_z}\,(z/L_{\frac{1}{2}}). \quad \text{(A-1c)}$$

$$z_{wD} = \sqrt{k_x/k_z}\,(z_w/L_{\frac{1}{2}}) \quad \text{(A-2a)}$$

and

$$h_D = \sqrt{k_x/k_z}\,(h/L_{\frac{1}{2}}). \quad \text{(A-2b)}$$

$$t_D = k_x t/\phi\mu c_t L_{1/2}^2 \quad \text{(A-3a)}$$

and $$s_D = \phi\mu c_t L_{1/2}^2 s/k_x. \quad \text{(A-3b)}$$

In these variables, the diffusion equation is that of an isotropic formation with unit diffusion coefficient:

$$\frac{\partial p}{\partial t_D} = \frac{\partial^2 p}{\partial x_D^2} + \frac{\partial^2 p}{\partial y_D^2} + \frac{\partial^2 p}{\partial z_D^2}. \quad \text{(A-4)}$$

For drawdown at constant rate q, we define a dimensionless pressure field p_D by

$$\Delta p = \frac{\mu}{2\pi\sqrt{k_x k_y}} \frac{q}{h} p_D(x_D, y_D, z_D, t_D; z_{wD}, h_D). \quad \text{(A-5)}$$

The boundary condition at the well is the infinite-conductivity condition that the pressure is uniform over the sandface. This poses a very difficult boundary-value problem. Thus, the actual solution we use is that of a uniform-flux line source. The chief theoretical difficulty is not how to write down this solution, but rather how best to use it to estimate the pressure at the sandface in the true infinite-conductivity case. If the well is long compared with its radius, then the problem in the transverse y and z directions may be decoupled from that in the longitudinal x direction.

Transverse Direction. In the above transformed coordinates the original circular well occupies the elliptical cylinder

$$\frac{(z_D - z_{wD})^2}{a_{wD}^2} + \frac{y_D^2}{b_{wD}^2} \le 1, \quad -1 < x_D < 1, \quad \text{(A-6)}$$

where $$a_{wD} = \sqrt{k_x/k_z}\,(r_w/L_{1/2}) \quad \text{(A-7a)}$$

and $$b_{wD} = \sqrt{k_x/k_y}\,(r_w/L_{1/2}). \quad \text{(A-7b)}$$

From the work of Kucuk and Brigham[6] and Muskat,[13] it is known that, when the flow near the well becomes pseudosteady, an elliptical well with semiaxes a and b in an isotropic formation is equivalent to a circular well of radius $\frac{1}{2}(a+b)$. Thus, in the dimensionless isotropic coordinate system, the correct equivalent dimensionless wellbore radius is

$$r_{wD} = \frac{a_{wD} + b_{wD}}{2} = \frac{r_w}{2L_{1/2}}\left(\sqrt{\frac{k_x}{k_y}} + \sqrt{\frac{k_x}{k_z}}\right). \quad \text{(A-8)}$$

Longitudinal Direction. The conventional method for use of the uniform-flux solution to approximate the infinite-conductivity solution is to use an equivalent pressure point; i.e., to evaluate the pressure at $x_D = x_D^*$, where x_D^* is some suitably chosen value. This approach was first proposed (for partially penetrating vertical wells) by Muskat,[13] who suggested the value $x_D^* = 0.75$, and studied in more detail by Gringarten and Ramey,[14] who gave values of x_D^* for a well in an infinite isotropic medium for various values of $r_w/L_{1/2}$. Here we will use an alternative method in which the pressure in the uniform-flux solution is averaged along the well length. This method has recently been discussed in detail by Wilkinson and Hammond,[12] who suggest (though do not rigorously prove) that it becomes exact in the limit of vanishingly small wellbore radius. We prefer this method for several reasons.

1. The pressure-averaging method requires no *a priori* information. While in principle the equivalent pressure-point method is exact at late times, the location of the pressure point depends on the geometry of the problem, i.e., not only on the ratio $r_w/L_{1/2}$ but also on the anisotropy in the transverse directions and the location of reservoir boundaries. Thus, the location of the pressure point must be determined anew for each problem, which can only be achieved by numerical solution of the original infinite-conductivity problem. By contrast, the pressure-averaging method always accounts for the geometry of the problem at hand, in a way that we believe is exact in the limit of vanishing wellbore radius.

2. An argument often advanced for the correctness of the equivalent-pressure-point method is that (provided that the point is correctly chosen) it is exact at late times, when the flow has become pseudosteady, and also at very early times, when the true solution has uniform flux and pressure. Hence it is reasonable to assume that it is correct also at intermediate times. This is very clearly not true. This is most easily seen by examining the instantaneous Green's function (dimensionless pulse response) for a finite uniform-flux line source in an infinite medium:

$$G(x_D, t_D) = \frac{1}{4\pi t_D} G_x(x_D, t_D) \exp\frac{-r_{wD}^2}{4t_D}, \quad \text{(A-9)}$$

where (see Appendix B)

$$G_x(x_D, t_D) = \frac{1}{4}\left(\operatorname{erf}\frac{1 - x_D}{\sqrt{4t_D}} + \operatorname{erf}\frac{1 + x_D}{\sqrt{4t_D}}\right). \quad \text{(A-10)}$$

Note that for small t_D, the quantity $G_x(x_D, t_D) = \frac{1}{2}$, and the solution is just that of a fully penetrating line source. Because the corrections to this limiting form are exponential in character, if we simply evaluate G_x at $x_D = x_D^*$, the solution will continue to look like a fully penetrating line source until dimensionless times of order $(1 - x_D^*)^2$, the pressure-diffusion time to the well end nearest the pressure point. This is not physically correct—the onset of deviation from the fully penetrating solution should be felt not suddenly but gradually, as the realization that the well is finite in length spreads in from the well ends. This effect is automatically accounted for in the pressure-averaging method in which G_x becomes

$$G_x(t_D) = \frac{1}{2}\int_{-1}^{1} dx_D G_x(x_D, t_D)$$

$$= \frac{1}{2}\left[\operatorname{erf}\frac{1}{\sqrt{t_D}} + \sqrt{\frac{t_D}{\pi}}\left(\exp\frac{-1}{t_D} - 1\right)\right]$$

$$\approx \frac{1}{2}\left[1 - \sqrt{\frac{t_D}{\pi}}\right], \quad \text{(A-11)}$$

as $t_D \to 0$; i.e., the deviation from the fully penetrating solution is algebraic. Assuming that the pressure-averaging solution is exact in the limit of small wellbore radius, the equivalent-pressure-point method overestimates the pressure response at intermediate times.

3. In a pressure test of a long horizontal well, the dimensionless time, t_D, may never become large, so the flow is never pseudosteady on the scale of the well length even at the end of the test. This is another drawback of the use of the equivalent pressure point, which is chosen to give the final pseudosteady pressure drop correctly.

Appendix B–Solutions

We develop our solutions using the instantaneous Green's function approach of Gringarten and Ramey.[5] This method has been used for the horizontal-well problem by Clonts and Ramey[3] and Ozkan *et al.*[4] Our solution differs from these works, however, because we use pressure averaging rather than equivalent pressure point, and we use the correct equivalent wellbore radius in anisotropic formations. For convenience in this section, we use the dimensionless variables given by Eqs. A-1 through A-3, but we drop the subscript D.

The instantaneous Green's function for the uniform-flux line source may be written as the product

$$G(x,y,z,t) = G_x(x,t) G_y(y,t) G_z(z,t). \quad \text{(B-1)}$$

Different forms of the solution may be obtained depending on whether we use Fourier series (or integral) techniques in each of the three directions.

In the x direction we have the response of a uniform-slab source occupying the region $-1 \le x \le 1$:

$$G_x(x,t) = \frac{1}{2}\int_{-1}^{1} dx' \frac{1}{2\sqrt{\pi t}} \exp[-(x - x')^2/(4t)]$$

$$= \frac{1}{4}\left[\operatorname{erf}\left(\frac{1 - x}{\sqrt{4t}}\right) + \operatorname{erf}\left(\frac{1 + x}{\sqrt{4t}}\right)\right]. \quad \text{(B-2)}$$

Alternatively, we may use the Fourier integral representation to obtain

$$G_x(x,t)=\frac{1}{2}\int_{-1}^{1}dx'\frac{1}{\pi}\int_0^\infty du\cos u(x-x')\exp(-u^2t)$$

$$=\frac{1}{\pi}\int_0^\infty du\cos ux\frac{\sin u}{u}\exp(-u^2t). \quad \text{(B-3)}$$

In the y direction, we have a sheet source located at $y=0$:

$$G_y(y,t)=\frac{1}{2\sqrt{\pi t}}\exp[-y^2/(4t)]. \quad \text{(B-4)}$$

In the z direction, we have a sheet source at $z=z_w$ with a no-flow lower boundary at $z=0$ and either a no-flow or uniform-pressure upper boundary at $z=h$. The solution may be written either as a Fourier series, as in Refs. 3 and 4, or as a sum over images. In the Fourier series representation, we have

$$G_z(z,t)=\frac{1}{h}\left[1+2\sum_{j=1}^{\infty}\cos\frac{j\pi z}{h}\cos\frac{j\pi z_w}{h}\exp\frac{-j^2\pi^2t}{h^2}\right], \quad \text{(B-5)}$$

for the no-flow upper-boundary case, and

$$G_z(z,t)=\frac{2}{h}\sum_{j=1}^{\infty}\cos\frac{(j-\frac{1}{2})\pi z}{h}\cos\frac{(j-\frac{1}{2})\pi z_w}{h}\times\exp\frac{-(j-\frac{1}{2})^2\pi^2t}{h^2}, \quad \text{(B-6)}$$

for the constant-pressure upper-boundary case. In the image-sum representation these solutions become

$$G_z(z,t)=\frac{1}{2\sqrt{\pi t}}\sum_{n=-\infty}^{\infty}(-1)^n\left[\exp\frac{-(z-z_w+2nh)^2}{4t}+\exp\frac{-(z+z_w+2nh)^2}{4t}\right], \quad \text{(B-7)}$$

where the factor $(-1)^n$ is absent in the case of the no-flow upper boundary. The equivalence of the Fourier and image-sum representations is expressed through the Poisson summation formula. For reasons of computational efficiency, it is clearly preferable to use the Fourier representation for large t (say $t>h^2$) and the image sum for small t (say $t<h^2$).

The above is the solution for a uniform-flux line source. To obtain the pressure at the well, we have to decide where to evaluate it. We use $G_x(t)$, $G_y(t)$, and $G_z(t)$ to denote the analogs of $G_x(x,t)$, $G_y(y,t)$, and $G_z(z,t)$ at the well. In the x direction, we use pressure averaging to obtain

$$G_x(t)=\frac{1}{2}\int_{-1}^{1}dxG_x(x,t)$$

$$=\frac{1}{2}\left[\operatorname{erf}\frac{1}{\sqrt{t}}+\sqrt{\frac{t}{\pi}}\left(\exp\frac{-1}{t}-1\right)\right]. \quad \text{(B-8)}$$

In the Fourier integral representation, this becomes

$$G_x(t)=\frac{1}{\pi}\int_0^\infty du\frac{\sin^2 u}{u^2}\exp(-u^2t). \quad \text{(B-9)}$$

In the y and z directions, according to the discussion of Appendix A, we should evaluate the pressure at an effective well radius r_w; i.e., somewhere on $y^2+(z-z_w)^2=r_w^2$. For a line source in an infinite isotropic medium, all such locations are equivalent, but in the presence of boundaries, there will be small, but unimportant, differences. We will make the choice $y=0$, $z=z_w+r_w$ so that

$$G_y(t)=G_y(y=0,t)=1/2\sqrt{\pi t} \quad \text{(B-10)}$$

and $$G_z(t)=G_z(z=z_w+r_w,t). \quad \text{(B-11)}$$

In Eq. B-11, $G_z(t)$ is obtained from Eq. B-5, B-6, or B-7, depending on the boundary condition at the top of the reservoir.

A major goal of this paper is to compute the Laplace transform $\hat{p}_D(s)$ of the dimensionless constant-rate response $p_D(t)$. This is related to $G(t)$ by

$$\hat{p}_D(s)=\frac{2\pi h}{s}\int_0^\infty dtG(t)e^{-st} \quad \text{(B-12)}$$

We may evaluate this Laplace transform in one of two ways, the first of which computes the Laplace integral numerically and the second analytically.

Numerical Laplace Transform. Computationally, we have found it most efficient to evaluate $G(t)=G_x(t)G_y(t)G_z(t)$ with the above formulas and then to compute the Laplace transform by numerical quadrature. Note that if we use Eq. B-8 for $G_x(t)$, then both $G_x(t)$ and $G_y(t)$ are simple to compute, while by appropriate choice of the Fourier (Eq. B-5 or B-6) or image-sum (Eq. B-7) representations, the function $G_z(t)$ can also be evaluated very quickly.

Analytical Laplace Transform. If we choose the Fourier integral representation (Eq. B-9) for $G_x(t)$ and the Fourier series representation (Eq. B-5 or B-6) to evaluate $G_z(t)$, then the Laplace integral may be done analytically. If we introduce the function

$$F(\beta)=\int_0^\infty\frac{\sin^2(u)du}{u^2(u^2+\beta)^{1/2}},$$

we find $$\hat{p}_D(s)=\frac{1}{s}F(s)+\frac{2}{s}\sum_{j=1}^{\infty}F\left[s+\left(\frac{j\pi}{h}\right)^2\right]\times\cos\left(\frac{j\pi z_w}{h}\right)\cos\left(\frac{j\pi z}{h}\right) \quad \text{(B-13)}$$

for the no-flow upper-boundary case, and

$$\hat{p}_D(s)=\frac{2}{s}\sum_{j=1}^{\infty}F\left[s+\frac{\pi^2(2j-1)^2}{4h^2}\right]\cos\left[\frac{(2j-1)\pi z_w}{2h}\right]\times\cos\left[\frac{(2j-1)\pi z}{2h}\right] \quad \text{(B-14)}$$

for the constant-pressure upper-boundary case. In both Eqs. B-13 and B-14, z should be set equal to z_w+r_w.

A useful feature of this solution approach is that, provided that the function $F(\beta)$ can be efficiently computed, it requires only the summing of a single series, which makes it most suitable for use on a vector computer, where the series can be summed in a single operation. If we represent the quantity $F(\beta)$ as an integral in the complex plane and evaluate it along the imaginary axis, we find

$$F(\beta)=\frac{\pi}{2\sqrt{\beta}}-\frac{1}{2\beta}+\frac{K_{i2}(2\sqrt{\beta})}{2\beta}, \quad \text{(B-15)}$$

where $$K_{i2}(\beta)=\int_0^\infty\frac{\exp(-\beta\cosh u)du}{\cosh^2 u}. \quad \text{(B-16)}$$

The function K_{i2} may be represented by Chebychev polynomials for computational efficiency.

In Eqs. B-13 and B-14 we can take the limit $s\to 0$ and determine the skin caused by the partial penetration effect, S_z, and the steady-

Authors

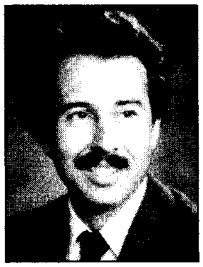
Kuchuk


Wilkinson

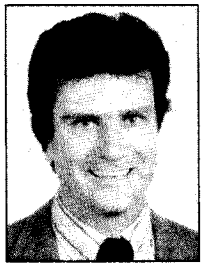
Goode

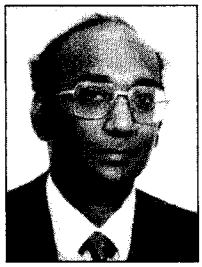
Thambynayagam

Fikri J. Kuchuk, a senior scientist and group leader at Schlumberger-Doll Research Center in Ridgefield, CT, researches fluid dynamics in porous media and performs reservoir tests. He has worked in the operation and engineering centers for Schlumberger in Paris and Houston and for Sohio Petroleum Co. in San Francisco. Kuchuk holds an MS degree from the Technical U. of Istanbul and MS and PhD degrees from Stanford U., all in petroleum engineering. **Peter A. Goode** is a research scientist at Schlumberger-Doll Research Center. Previously, he was a senior reservoir engineer with Sohio Petroleum Co. and Santos Ltd. in South Australia. He holds a BS degree in mathematics from the U. of Adelaide. **David J. Wilkinson** is a senior research scientist at Schlumberger-Doll Research Center. He joined Schlumberger in 1981 and works on fluid flow in porous media. Wilkinson holds a BA degree in pure and applied mathematics from Trinity C., Cambridge, and a PhD degree in theoretical physics from the U. of Pennsylvania. **R.K.M. Thambynayagam** is manager of interpretation engineering at Schlumberger Well Services in Houston. He has also worked for Sohio in San Francisco and for BP Petroleum Co. in London. Thambynayagam researches process, petroleum, and reservoir engineering. He holds a PhD degree in chemical engineering from the U. of Manchester, U.K.

state pressure, p_{ss}, respectively. For small s we may show that

$$F(s) \approx -\tfrac{1}{2}\ln(s) + \tfrac{3}{2} - \gamma. \quad \text{(B-17)}$$

For the no-flow upper-boundary case, we find that for large t,

$$p_D(t) \approx \tfrac{1}{2}[\ln(t) + 2.4228] + S_z, \quad \text{(B-18)}$$

where

$$S_z = -\frac{h}{2}\ln\left[\frac{2\pi r_w}{h}\sin\left(\frac{\pi z_w}{h}\right)\right] - \frac{h}{2}\left(\frac{h}{3} - z_w + \frac{z_w^2}{h}\right) + \frac{h^2}{\pi^2}\sum_{j=1}^{\infty}\frac{1}{j^2}K_{i2}\left(\frac{2j\pi}{h}\right)\cos^2\left(\frac{j\pi z_w}{h}\right). \quad \text{(B-19)}$$

For $h < 5$, as is generally the case in practice, the summation term is negligible and we obtain simply

$$S_z \approx -\frac{h}{2}\ln\left[\frac{2\pi r_w}{h}\sin\left(\frac{\pi z_w}{h}\right)\right] - \frac{h}{2}\left(\frac{h}{3} - z_w + \frac{z_w^2}{h}\right). \quad \text{(B-20)}$$

The steady-state pressure for the constant-pressure boundary-condition case can be developed from Eq. B-14 in a similar manner.

$$p_{ss} = \frac{h}{2}\ln\left[\frac{4h}{\pi r_w}\cot\left(\frac{\pi z_w}{2h}\right)\right] - \frac{h}{2}(h - z_w) + \frac{h^2}{\pi^2}\sum_{j=1}^{\infty}\frac{4}{(2j-1)^2}K_{i2}\left[\frac{(2j-1)\pi}{h}\right]\cos^2\left[\frac{(2j-1)\pi z_w}{2h}\right]. \quad \text{(B-21)}$$

For $h < 2.5$, the summation term is negligible and we obtain simply

$$p_{ss} \approx \frac{h}{2}\ln\left[\frac{4h}{\pi r_w}\cot\left(\frac{\pi z_w}{2h}\right)\right] - \frac{h}{2}(h - z_w). \quad \text{(B-22)}$$

SI Metric Conversion Factors

ft	× 3.048*	E−01 = m
md	× 9.869 233	E−04 = μm^2

*Conversion factor is exact.

SPEFE

Original SPE manuscript received for review March 23, 1988. Paper accepted for publication Oct. 1, 1990. Revised manuscript received Aug. 17, 1990. Paper (SPE 17413) first presented at the 1988 SPE California Regional Meeting held in Long Beach, March 23–25.